Beyond-Hubbard Pairing in a Cuprate Ladder

Hari Padma,[1,‡] Jinu Thomas,[2,3] Sophia F. R. TenHuisen,[1,4] Wei He,[5] Ziqiang Guan,[1] Jiemin Li,[6] Byungjune Lee,[7,8] Yu Wang,[9,10] Seng Huat Lee,[9,10] Zhiqiang Mao,[9,10] Hoyoung Jang,[11] Valentina Bisogni,[6] Jonathan Pelliciari,[6] Mark P. M. Dean,[5] Steven Johnston,[2,3,*] and Matteo Mitrano[1,†]

[1]*Department of Physics, Harvard University, Cambridge, Massachusetts, USA*
[2]*Department of Physics and Astronomy, University of Tennessee, Knoxville, Tennessee, USA*
[3]*Institute of Advanced Materials and Manufacturing, University of Tennessee, Knoxville, Tennessee, USA*
[4]*John A. Paulson School of Engineering and Applied Sciences, Harvard University, Cambridge, Massachusetts, USA*
[5]*Condensed Matter Physics and Materials Science Department, Brookhaven National Laboratory, Upton, New York, USA*
[6]*National Synchrotron Light Source II, Brookhaven National Laboratory, Upton, New York, USA*
[7]*Department of Physics, Pohang University of Science and Technology, Pohang, Korea*
[8]*Max Planck POSTECH/Korea Research Initiative, Center for Complex Phase Materials, Pohang, Korea*
[9]*2D Crystal Consortium, Materials Research Institute, Pennsylvania State University, University Park, Pennsylvania, USA*
[10]*Department of Physics, Pennsylvania State University, University Park, Pennsylvania, USA*
[11]*PAL-XFEL, Pohang Accelerator Laboratory, POSTECH, Pohang, Korea*

(Received 15 January 2025; revised 19 March 2025; accepted 10 April 2025; published 12 May 2025)

The Hubbard model is believed to capture the essential physics of cuprate superconductors. However, recent theoretical studies suggest that it fails to reproduce a robust and homogeneous superconducting ground state. Here, using resonant inelastic x-ray scattering and density matrix renormalization group calculations, we show that magnetic excitations in the prototypical cuprate ladder $Sr_{14}Cu_{24}O_{41}$ are inconsistent with those of a simple Hubbard model. The magnetic response of hole carriers, contributing to an emergent branch of spin-flip excitations, is strongly suppressed. This effect is the consequence of strong *d*-wavelike pairing, enhanced by nearly an order of magnitude through a large nearest-neighbor attractive interaction and persisting up to at least 260 K. The close connection between the physics of cuprate ladders and that of the two-dimensional compounds suggests that such an enhanced hole pairing may be a universal feature of superconducting cuprates.

DOI: 10.1103/PhysRevX.15.021049

Subject Areas: Condensed Matter Physics

Understanding how electrons pair in strongly correlated materials such as the cuprate superconductors is a major unsolved problem in condensed matter physics [1,2]. While pairing in conventional superconductors occurs via electron-phonon interaction, the pairing mechanism and onset of superconductivity in the presence of strong electron-electron interactions is a correlated many-body problem that presents additional challenges. The single-band Hubbard model, where electrons in a lattice hop with a characteristic energy t and interact through an on-site Coulomb repulsion U, is widely regarded as the minimal description of the cuprates [2,3]. This model successfully captures the presence of antiferromagnetism, charge order, a pseudogap, and a Fermi-liquid-like regime [2,4–7]. However, it is unclear whether the Hubbard model alone yields a robust *d*-wave superconducting ground state over competing spin- and charge-ordered phases [8–10]. Furthermore, recent calculations suggest that its low-energy antiferromagnetic spin fluctuations can only account for half of the total pairing interaction [11]. Together with the pronounced sensitivity of superconductivity to band structure effects [12] and additional interactions [13–17], these findings strongly suggest that the Hubbard model provides an incomplete description of cuprate superconductivity.

Since antiferromagnetic correlations play a crucial role in the behavior of the high-T_c cuprates, a powerful strategy to shed light on missing many-body interactions is to probe their magnetic excitation spectrum and compare it with the predictions of different model Hamiltonians. Cuprate ladders [see Fig. 1(a)] are uniquely well suited to this endeavor [18,19]. Unlike their two-dimensional counterparts, cuprate ladders can be accurately described using

*Contact author: sjohn145@utk.edu
†Contact author: mmitrano@fas.harvard.edu
‡Contact author: hpadmanabhan@g.harvard.edu

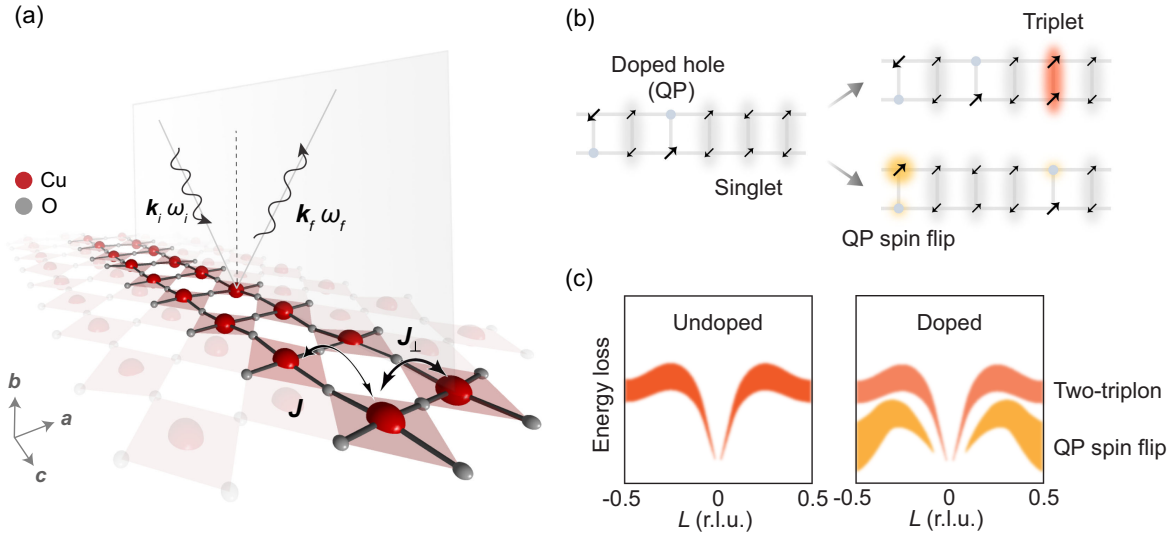

FIG. 1. Magnetic excitations of the cuprate ladder $Sr_{14}Cu_{24}O_{41}$. (a) Sketch of resonant inelastic x-ray scattering off the cuprate ladder compound $Sr_{14}Cu_{24}O_{41}$. The ladder legs and rungs run parallel to the c and a axes, respectively. The scattering plane is spanned by the sample b and c axes. J and $J_\perp$ indicate the exchange couplings along the "leg" and "rung" directions, respectively. $\boldsymbol{k}_i$ ($\boldsymbol{k}_f$) and ω_i (ω_f) denote initial (final) momentum and energy of the x-ray photons. (b) A hole-doped spin ladder features loosely bound quasiparticles (QP) in a background of spin singlets. There are two types of magnetic excitations with $\Delta S = 1$: singlet-to-triplet excitations and quasiparticle spin flips. Black arrows and gray and yellow circles represent spins and holes, while gray and red shadings correspond to spin singlets and triplets, respectively. Singlet correlations along the legs are omitted for simplicity. (c) Expected dispersions of two-triplon (orange) and QP spin-flip excitations (yellow) along the leg direction in an undoped (left) and hole-doped (right) ladder (for $H = 0$). Momenta are labeled in reciprocal lattice units (r.l.u.).

modern density matrix renormalization group (DMRG) methods and their magnetic excitations can be computed with excellent energy and momentum resolution. At the same time, these systems retain the key properties of the high-T_c superconducting compounds, including charge order [20] and superconductivity [21,22]. Further, the CuO_2 planes in the presence of charge stripes in the 2D high-T_c cuprates have previously been modeled in terms of coupled ladders [23,24] with magnetic excitations that could explain the "hourglass" dispersion observed in underdoped compounds [25,26]. These features highlight the deep connection between the physics of ladder compounds and that of two-dimensional cuprates [27], and establish ladder systems as promising platforms to shed light on Cooper pairing in higher-dimensional cuprate families.

The magnetic excitation spectrum of cuprate ladders is theoretically known to be sensitive to both the underlying electronic interactions and the presence of doped carriers. The ground state of an isotropic, undoped ladder consists of spin singlets [28] and its elementary magnetic excitations are singlet-to-triplet transitions ["triplons"; see Fig. 1(b)]. Each doped hole breaks a spin singlet and behaves like a quasiparticle with loosely bound spin and charge components [29,30], which contribute distinct spin-flip excitations [29,31]. As sketched in Fig. 1(c) (for $H = 0$, see the Appendix), the magnetic excitation spectrum of an undoped Hubbard ladder features a continuum of two-triplon excitations, whereas a doped ladder exhibits an additional branch of quasiparticle spin flips just below the continuum. Resolving these two broad features is technically challenging and requires high spectral resolution and counting statistics. As a result, the identification of magnetic excitations arising from doped carriers in cuprate ladders has remained elusive.

Here, we report high-resolution (~35 meV) Cu L_3-edge resonant inelastic x-ray scattering (RIXS) measurements of the magnetic excitations in the cuprate ladder $Sr_{14}Cu_{24}O_{41}$. In this compound, the ladders are self-doped with ~0.06 holes/Cu atom [19,32,33], which form a charge-ordered state [20] below T_{CO} of 250 K [see Supplemental Material (SM) Sec. I [34]]. The presence of self-doped holes in the parent compound provides a unique opportunity to probe the magnetic excitations of the doped holes without the added complexity of chemical substitution. The raw RIXS spectra measured at 260 K [Fig. 2(a); see SM Sec. II for raw RIXS spectra at 40 K [34]] along the leg direction show peaks corresponding to the elastic line, a 60-meV bond-stretching phonon, its second harmonic, and dispersive magnetic excitations with spectral weight up to 600 meV. We isolate the magnetic excitations by fitting and subtracting elastic and phonon contributions as shown in Fig. 2(b) (see SM Sec. S2 for fit details). We then normalize the subtracted spectra using the intensity of the *dd* orbital excitations and the spin-flip scattering cross section calculated using a single-ion model [35,36]. This procedure yields the dynamical spin structure factors

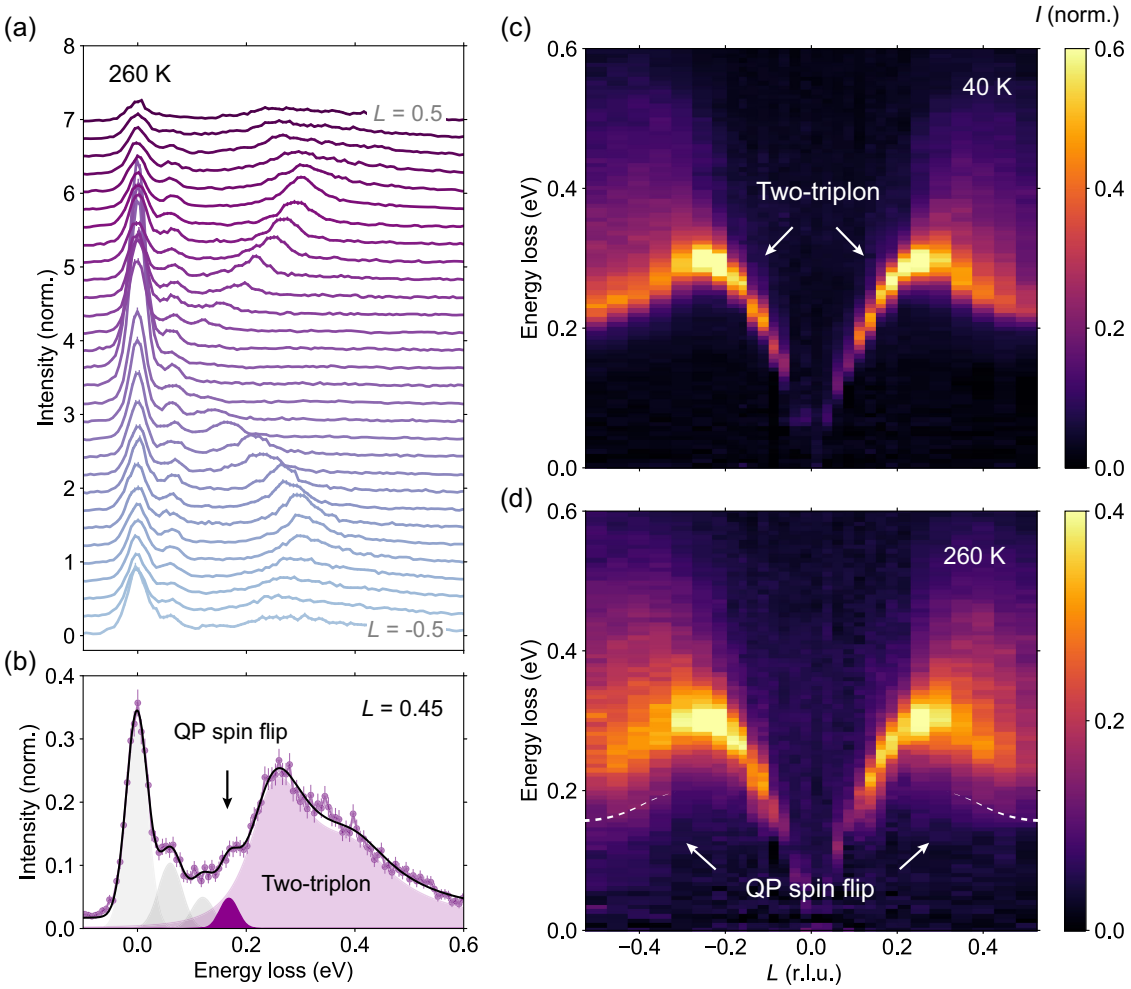

FIG. 2. Magnetic excitations from the doped holes. (a) RIXS spectra along the leg direction for momenta spanning $L = -0.5$–0.5 r.l.u., measured at 260 K. Spectra are vertically offset for clarity. (b) Representative fit to the low-energy region of the RIXS spectrum ($L = 0.45$ r.l.u.) at 260 K (solid line), with the elastic peak, bond-stretching phonon, and its second harmonic fit to Gaussians, shaded in light gray. The quasiparticle spin-flip feature is fit to a Gaussian, shaded in dark pink. The two-triplon continuum is fit to a phenomenological line shape consisting of an asymmetric Lorentzian and a Gaussian, shaded in light pink. (c),(d) Intensity map of the dynamical spin structure factor at 40 and 260 K (below and above the charge order transition, respectively) as function of momentum and energy loss. We subtract elastic and phonon contributions, shown in (b), and normalize the data to the orbital excitation and spin-flip scattering cross section as described in the SM [34]. While the map at 40 K exhibits negligible spectral weight below the two-triplon continuum, the map at 260 K features an additional weak branch corresponding to quasiparticle spin-flip excitations. The dashed white lines are a guide to the eye. The energy resolution of our RIXS measurement is ∼35 meV.

shown in Figs. 2(c) and 2(d) (see SM Sec. II for further details). The magnetic excitations are dominated by an intense two-triplon continuum, with a shape and dispersion consistent with previous experimental and theoretical results [29,31,37,38].

We now discuss the key spectroscopic feature of this work. By leveraging our high-energy resolution, we detect a previously unobserved dispersive magnetic peak below the two-triplon continuum, near the zone boundary [Figs. 2(b) and 2(d); see additional momenta in SM Sec. II [34]]. Its dispersion closely follows the low-energy shoulder of the two-triplon continuum, consistent with the expected behavior of the quasiparticle spin-flip branch [29,31]. We confirm the spin-flip character of this excitation by examining its θ dependence (see SM Sec. II and Fig. S9). However, its intensity is strongly suppressed compared to theoretical expectations for a doped Hubbard ladder [29,31]. The quasiparticle spin-flip branch is completely absent at low temperature ($T < T_{CO}$), and only faintly present in the high-temperature spectra ($T > T_{CO}$), as shown in Figs. 2(b) and 2(d). While the absence of the quasiparticle spin-flip branch at low temperature might be associated with the opening of the charge order gap, this cannot explain its weak intensity above T_{CO}. Disorder alone, which can pin holes to the lattice and modify the spin-flip spectral weight, may also be ruled out as a dominant factor. A previous study on the Ca-doped compound [38] showed that the disordered Hubbard model

predicts a broadened and flattened dispersion of the two-triplon continuum. In contrast, the parent compound we consider here is not disordered by chemical substitution and exhibits a well-defined and strongly dispersive two-triplon continuum.

We investigate the origin of this intensity discrepancy by comparing the RIXS data with DMRG calculations of the dynamical spin structure factor of a single-band Hubbard ladder. We first extract the parameters of the undoped Hubbard ladder by fitting the experimental two-triplon dispersion at 40 K using a Bayesian optimization procedure (see the Appendix). We obtain a nearest-neighbor leg hopping $t = 0.38$ eV, rung hopping $t_\perp = 0.84t$, a diagonal hopping $t' = -0.3t$, and an on-site Coulomb repulsion $U = 8t$. The corresponding superexchange interactions are $J = -4t^2/U = 190$ meV and $J_\perp = -4t_\perp^2/U = 134$ meV, which are in excellent agreement with reported values extracted from inelastic neutron scattering [39]. We then use these parameters to calculate the dynamical spin structure factor of the two-leg Hubbard ladder upon 6.25% hole doping [32,33] using the Krylov space correction vector method [40] (see SM Sec. III [34]). As shown in Fig. 3(a), the DMRG spectra feature an intense branch of quasiparticle spin flips with a downward dispersion at the Brillouin zone boundary. This result is consistent with prior calculations [31], but is in stark contrast with the measured magnetic spectra. We note that the three-band Hubbard model also cannot account for our experimental data. Prior work shows that the doped low-energy magnetic excitation spectra of the three-band model are nearly identical to their effective single-band counterparts [41].

Such a disagreement suggests the presence of additional interactions suppressing the free propagation of spin-1/2 quasiparticles that would otherwise disrupt the singlet background. Since the simple Hubbard model assumes only an on-site Coulomb repulsion, which might not sufficiently account for nonlocal interactions, we consider the effect of an additional nearest-neighbor Coulomb interaction V. A repulsive interaction ($V > 0$) does not significantly alter the calculated spin structure factor (see SM Fig. S10 [34]). However, the introduction of a nearest-neighbor attraction ($V < 0$) dramatically suppresses the intensity of the quasiparticle spin-flip excitations and sharpens the two-triplon continuum. We obtain the best agreement between experiment and DMRG calculations by introducing an attractive interaction V of order $-1.0t$ to $-1.25t$ [see Figs. 3(b) and 3(c)]. A closer inspection of the DMRG spectra at selected momenta, presented in Figs. 3(d) and 3(e), reveals that the suppression of magnetic excitations from the doped holes is monotonic with increasing V. An angle-resolved photoemission spectroscopy (ARPES) study of holon states in the nonsuperconducting chain compound $Ba_{2-x}Sr_xCuO_{3+\delta}$ obtained a very similar value of V, in the range $-0.8t$ to $-1.2t$ [42]. The agreement between our results on a ladder system, which becomes superconducting under doping, and findings in doped one-dimensional chains supports the notion that this interaction is robust and occurs in superconducting cuprate families with higher dimensionality. Such an attractive interaction has been posited to arise from electron-phonon coupling [42,43], which is known to be significant in two-dimensional cuprates [44,45] as well as cuprate ladders [46]. Alternatively, an effective attractive interaction between doped holes could also emerge from the nonuniform electric polarizability of the system [47].

Next, we examine the effect of this nearest-neighbor attraction on the magnetic excitations by analyzing its influence on holes. Figure 3(f) illustrates that in an isotropic Hubbard ladder (where $V = 0$), doped holes disrupt rung singlets. These holes are weakly paired, with a correlation length of 2–3 lattice constants for model parameters consistent with $Sr_{14}Cu_{24}O_{41}$ [28,29]. Introducing a negative V makes it energetically favorable for holes to form tightly bound pairs on the same rung. Consequently, more unbroken spin singlets are available for excitation into triplets, enhancing the intensity of the two-triplon excitations at the cost of the quasiparticle spin-flip continuum. That is, the suppression of the quasiparticle spin-flip branch is a direct consequence of enhanced hole pairing. Our DMRG calculations show that the attractive V enhances the hole-hole binding energy by almost an order of magnitude relative to the pure Hubbard model, with the value increasing to $0.074t$ for $V = -1.25t$ [see Fig. 3(f)].

Based on the intensity suppression observed above T_{CO}, we underscore that the enhanced hole pairing is present at temperatures above the onset of charge order and is not a consequence of the formation of a charge order gap. Importantly, while we illustrate hole pairs along the rungs for simplicity in Fig. 3(e), the attractive V in our model is isotropic along the leg and rung directions. Our calculations (see SM Fig. S11 [34]) show that the resulting pair-pair correlations for such an interaction retain the same quasi-d-wavelike structure as obtained for $V = 0$, where the pair correlations along the rung are opposite in sign to those along the leg despite the lack of local C_4 symmetry about each site. This conclusion is consistent with another recent study that examined a two-leg ladder with isotropic hopping [48].

Finally, we investigate the effective dimensionality of the ladder, and consider whether our observation of enhanced pairing due to a large attractive Coulomb interaction can be generalized to other cuprate families. In one-dimensional systems, electrons decouple into distinct collective excitations of spin (spinons), charge (holons), and orbital (orbitons) degrees of freedom, each propagating at different velocities. Spin-orbital separation enables orbitons to propagate coherently between neighboring sites, manifesting as a dispersive orbital excitation with periodicity π [49]. In contrast, orbitons in higher dimensions are constrained by magnetic interactions, making their dispersion a crucial

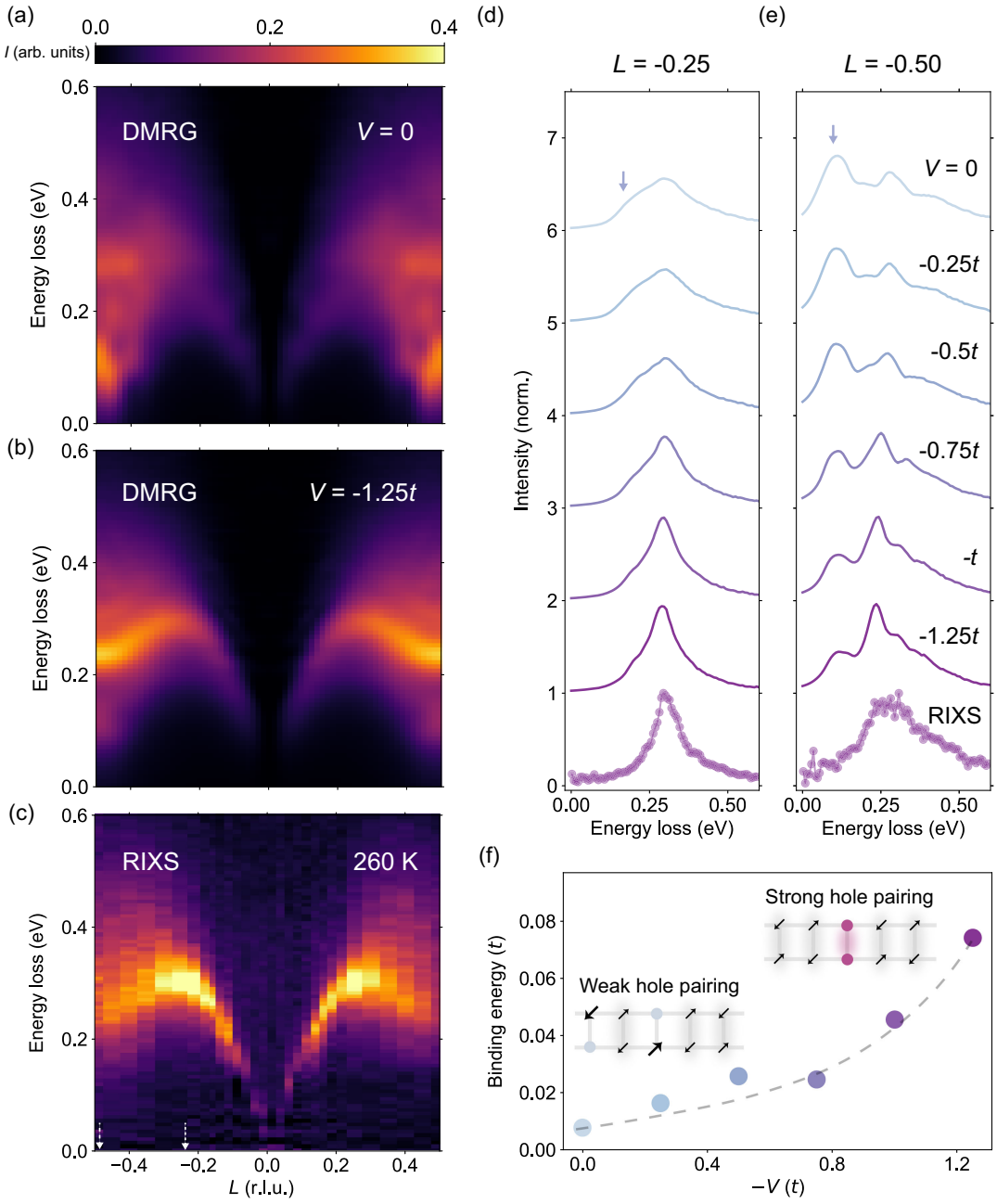

FIG. 3. Signatures of enhanced hole pairing due to an attractive nearest-neighbor interaction. (a),(b) Theoretical dynamical spin structure factors for $V = 0$ (a) and $-1.25t$ (b), calculated using DMRG on ladder clusters. (c) Experimental dynamical spin structure factor. White arrows indicate selected momenta shown in (d) and (e). (d),(e) Experimental (filled circles) and theoretical (solid lines) dynamical spin structure factors at $L = -0.25$ and -0.50 r.l.u.. DMRG curves for varying V are vertically offset for clarity. The best agreement between theory and experiment occurs for $V = -1.25t$. The pale blue arrows point to the quasiparticle spin-flip excitations. (f) The hole pair binding energy as a function of V. As $-V$ increases, holes tend to pair on neighboring sites. Arrows and circles represent spins and holes, respectively, while the purple shading represents the hole pair binding. The dashed line is a guide to the eye.

measure of electronic fractionalization and system dimensionality. In Fig. 4, we present evidence of spin-orbital separation in the RIXS spectra. The excitation of Cu $3d$ $x^2 - y^2$ holes into different orbital states gives rise to a manifold of transitions between 1.6 and 2.7 eV. We focus on the xz/yz feature, which displays a characteristic orbiton dispersion similar to that observed in corner-sharing cuprate chain compounds [49–51]. We note that our spectra are expected to contain a small, overlapping intensity contribution from the edge-sharing chains in $Sr_{14}Cu_{24}O_{41}$, which cannot be identified in our fits. Since the excitations from the chains are expected to show little to no dispersion

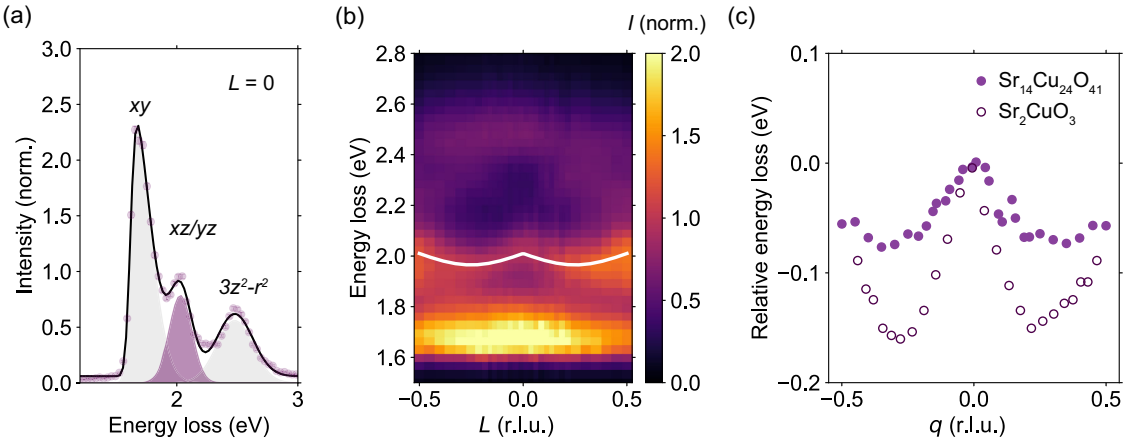

FIG. 4. Orbiton dispersion and dimensional crossover. (a) RIXS spectrum (circles) and fit (solid line) of the *dd* orbital excitations at $L = 0$. The fit includes three Lorentzian corresponding to excitations from the $3d\ x^2 - y^2$ orbital to xy (gray), xz/yz (purple), and $3z^2 - r^2$ (gray) orbitals. Note that here, x, y, and z are parallel to the crystallographic a, c, and b directions, respectively. (b) RIXS intensity map of the *dd* excitations as function of momentum and energy loss. The white solid line is a fit to the lower edge of the orbiton dispersion derived from the Kugel-Khomskii Hamiltonian with $J_O = (22.5 \pm 5.4)$ meV. (c) Orbiton dispersion in cuprates with varying dimensionality. The ladder data are a fit to the spectra shown in (b), while the data for the cuprate chain Sr_2CuO_3 are reproduced from Ref. [49].

(see SM Sec. II [34]), we omitted them from our analysis. This approximation is not expected to have a major effect on our extracted dispersion. The lower branch of the xz/yz orbiton in Fig. 4(b) is well described by the Kugel-Khomskii model [52] (see SM Sec. II for details). We obtain an effective orbital superexchange parameter $J_O = 22.5 \pm 5.4$ meV, which quantifies the propagation of orbital excitations along the ladder legs. This value is substantially lower than $J_O \sim 75$ meV found in Sr_2CuO_3 [49] and indicates a higher degree of orbiton confinement when compared to cuprate chains. We also note that the ladder orbiton superexchange is comparable to the 15 meV interaction recently measured in two-dimensional $CaCuO_2$ [53], where orbiton propagation with periodicity 2π is enabled by strong next-nearest-neighbor hopping due to the absence of apical oxygens.

Furthermore, the spin-orbital separation in $Sr_{14}Cu_{24}O_{41}$ is not accompanied by spin-charge separation [29,30], as evidenced by the gapped two-triplon continuum (see Fig. 2), which significantly departs from the gapless spinon dispersion observed in chain compounds [49] and extremely anisotropic ladders [54]. These observations place $Sr_{14}Cu_{24}O_{41}$ in a crossover regime between one and two dimensions and indicate that our findings may be directly relevant to the isotropic two-dimensional CuO_2 plane.

Our observation of enhanced hole pairing due to an attractive Coulomb interaction in a cuprate ladder has broader implications for the understanding of how superconductivity is stabilized in cuprates. On the one hand, our data indicate that an attractive intersite interaction may be a crucial addition to the minimal Hubbard model for cuprates beyond spin chain compounds. On the other hand, the large binding energy and the *d*-wave symmetry of the hole pairing, together with recent work on related theoretical models [14,16], suggest that an attractive V might be important in enhancing superconducting correlations over charge order and other symmetry breaking phenomena that dominate in a pure Hubbard model. Our work provides an experimental basis for what may be the key missing ingredient in the theoretical description of robust *d*-wave superconductivity in two-dimensional hole-doped cuprates and motivates the search for a similar minimal model in the electron-doped sector of the cuprate phase diagram.

Note added in proof. Recently, we became aware of an independent inelastic neutron scattering study on $Sr_{14-x}Ca_xCu_{24}O_{41}$ arriving at similar conclusions [55].

We thank P. Abbamonte, N. P. Armitage, C. D. Batista, E. Demler, M. Dressel, A. Georges, T. Giamarchi, S. A. Kivelson, A. J. Millis, S. Sachdev, M. Sentef, D. A. Tennant, and J. Tranquada for insightful discussions. This work was primarily supported by the U.S. Department of Energy, Office of Basic Energy Sciences, Early Career Award Program, under Award No. DE-SC0022883. The work by J. T. and S. J. (theory modeling) was supported by the U.S. Department of Energy, Office of Science, Office of Basic Energy Sciences, under Award No. DE-SC0022311. Work performed at Brookhaven National Laboratory (RIXS and RIXS data interpretation) was supported by the U.S. Department of Energy (DOE), Division of Materials Science, under Contract No. DE-SC0012704. B. L. and H. J. were supported by the National Research Foundation of Korea (MSIT), Grant No. 2022M3H4A1A04074153 and No. 2020M3H4A2084417. This research used resources

at the SIX beam line of the National Synchrotron Light Source II, a U.S. DOE Office of Science User Facility operated for the DOE Office of Science by Brookhaven National Laboratory under Contract No. DE-SC0012704. This research used TEM Sample Preparation Facilities of the Center for Functional Nanomaterials (CFN), which is a U.S. Department of Energy Office of Science User Facility, at Brookhaven National Laboratory under Contract No. DE-SC0012704. The work at the PAL-XFEL was performed at the RSXS end station (Proposal No. 2023-1st-SSS-002), funded by the Korea government (MSIT). The single crystal growth work was performed at the Pennsylvania State University Two-Dimensional Crystal Consortium–Materials Innovation Platform (2DCC-MIP), which is supported by NSF Cooperative Agreement No. DMR-2039351.

H. P., M. P. M. D., and M. M. conceived the experiment. H. P., S. T., W. H., Z. G., J. L., J. P., and V. B. conducted the RIXS measurements. J. T. and S. J. performed the DMRG calculations. H. P., S. T., B. L., and H. J. conducted the x-ray absorption spectroscopy and resonant soft x-ray diffraction measurements. Y. W., S. H. L., and Z. M. synthesized the single crystal samples. H. P. analyzed the data with assistance from M. P. M. D. H. P., M. P. M. D, S. J., and M. M. wrote the article with input from all authors. M. M. and S. J. supervised the experimental and theoretical aspects of the project, respectively.

DATA AVAILABILITY

The data that support the findings of this article are not publicly available. The data are available from the authors upon reasonable request.

APPENDIX: METHODS

1. Sample growth and characterization

High-quality single crystal samples of $Sr_{14}Cu_{24}O_{41}$ were grown using a modified traveling solvent floating zone (TSFZ) technique. We first synthesized pure polycrystalline $Sr_{14}Cu_{24}O_{41}$ powder via a solid-state reaction, which we used as a feed material rod. We then chose CuO as the flux during the TSFZ growth. The flux rod (seed) was prepared by mixing the $Sr_{14}Cu_{24}O_{41}$ and CuO powders with the mass ratio of $Sr_{14}Cu_{24}O_{41}$: CuO = 1:0.0163.

The feed speed of the feed rod was tuned within the 0.81–2.2 mm/h range to maintain stable growth, and the growth speed was 0.81 mm/h. Both feed and seed rods were rotated in mutually opposite directions at 30 rpm. We obtained a crystal rod with a length of 2 cm and a diameter of 4 mm. X-ray diffraction measurements confirmed good crystallinity and a structure in agreement with previous reports [56]. Characterization of the hole doping and charge order are provided in Supplemental Material (see Fig. S1 and S2) [34].

2. RIXS measurements

We conducted high-resolution RIXS measurements at the beam line 2-ID of the National Synchrotron Light Source II, Brookhaven National Laboratory. The incident x-rays were π polarized and tuned at resonance with the Cu L_3-edge peak (932.5 eV) with a combined energy resolution of 35 meV. We oriented a single crystal sample using Laue diffraction, which was then cleaved *in situ* and mounted with the b and c axes in the scattering plane for all measurements described in the main text, as shown in Fig. 1(a). The lattice parameters are $a = 11.47$ Å, $b = 13.35$ Å, and $c = 7c_L = 10c_C = 27.46$ Å, where the subscripts L and C represent the ladder and chain subunits, respectively [57] (see SM Sec. I for more details on crystal structure [34]). Our measurements are performed with the scattering angle fixed at 150°, while varying the incident angle θ by rotating the sample about the a axis from 12.9° to 137.1°, corresponding to momentum transfers of $L = -0.5$ to 0.5 r.l.u. (defined in units of $2\pi/c_L$), with $H = 0$. Given the layered crystal structure of $Sr_{14}Cu_{24}O_{41}$, we neglect the dispersion along the K direction.

The symmetry of the ladder geometry implies that sectors of even and odd triplon number do not mix, due to their different parity with respect to reflection about the centerline of the ladder [39]. Hence, one- and two-triplon contributions can be studied in isolation by measuring at $H = 0.5$ and $H = 0$, respectively. In particular, since H is fixed to zero, all measurements reported in the main text are sensitive to excitations with even triplon number, which is dominated by the two-triplon continuum. The raw RIXS spectra collected at 40 and 260 K are shown in Figs. S4 and S5, respectively [34]. We conducted an additional set of measurements with the a and b axes in the scattering plane to detect the one-triplon excitation. We collected spectra at $\theta = 74.6°$ and 10.9° corresponding to momenta of $H = 0$ and -0.5 (with $L = 0$). The spectra, presented in Fig. S7, show a one-triplon peak at an energy loss of 210 meV, consistent with previous inelastic neutron scattering measurements [39].

3. DMRG calculations

a. Model parameters

We simulate an extended Hubbard model on a two-leg ladder. The model Hamiltonian is

$$\begin{aligned} H = &-t\sum_{i,l,\sigma}(\hat{c}^{\dagger}_{i,l,\sigma}\hat{c}_{i+1,l,\sigma} + \text{H.c.}) - t_{\perp}\sum_{i,\sigma}(\hat{c}^{\dagger}_{i,1,\sigma}\hat{c}_{i,2,\sigma} + \text{H.c.}) \\ &- t'\sum_{i,\sigma}(\hat{c}^{\dagger}_{i,1,\sigma}\hat{c}_{i+1,2,\sigma} + \hat{c}^{\dagger}_{i,2,\sigma}\hat{c}_{i+1,1,\sigma} + \text{H.c.}) \\ &+ U\sum_{i,l}\hat{n}_{i,l,\uparrow}\hat{n}_{i,l,\downarrow} + V\sum_{\substack{\langle i,l,i',l'\rangle \\ \sigma,\sigma'}}\hat{n}_{i,l,\sigma}\hat{n}_{i',l',\sigma'}, \end{aligned} \tag{A1}$$

where $l = 1, 2$ indexes the ladder leg, and the index i runs over sites along the leg of length L. $\hat{c}^{\dagger}_{i,l,\sigma}$ ($\hat{c}_{i,l,\sigma}$) creates (annihilates) an electron at site i, l with spin σ. $\hat{n}_{i,l,\uparrow}$ ($\hat{n}_{i,l,\downarrow}$)

is the number of up (down) electrons, $\langle\cdots\rangle$ denotes a sum over nearest-neighbor sites along both the leg and rung directions, t and $t_\perp$ are the nearest-neighbor hopping parameters along the leg and rung directions, respectively, t' is the next-nearest-neighbor hopping along the diagonal direction of the ladder unit, U is the on-site Hubbard repulsion, and V is the nearest-neighbor Coulomb interaction.

Setting $t = 0.38$ eV and $U = 8t$, we tune for $t_\perp$ and t' by comparing the experimental two-triplon spectra at 40 K to calculations of $S(\boldsymbol{q},\omega)$ for undoped Hubbard ladders. V is only introduced later for the doped ladder calculations. Since the overall bandwidth of the two-triplon dispersion is controlled by exchange interaction $J = -4t^2/(U-V)$ along the leg, we adjusted the value of U once V is introduced to keep the value of J fixed.

For the ladder system, the dynamical spin structure factor is defined as

$$S(\boldsymbol{q},\omega) = \sum_{f,\sigma} |\langle\psi_f|\hat{S}^z_{\boldsymbol{q}}|\psi_0\rangle|^2 \delta(E_f - E_0 + \omega), \tag{A2}$$

where $S^z_{\mathbf{q}} = (1/\sqrt{2L})\sum_{i,l} e^{-i\mathbf{q}\cdot\mathbf{r}_{i,l}} S^z_{i,l}$ is the Fourier transform of the z component of the local spin operator, $\boldsymbol{q}$ and ω are the net momentum and energy transfer into the system, ψ_0 is the ground state with energy E_0, and f indexes all final states ψ_f with energy E_f. To compute $S(\mathbf{q},\omega)$, we work in real space and evaluate

$$S_{c,j}(\omega) = -\frac{1}{\pi}\mathrm{Im}\langle\Psi_0|\hat{S}^z_j \frac{1}{\omega - H + E_0 + i\eta}\hat{S}^z_c|\Psi_0\rangle \tag{A3}$$

using the Krylov space correction vector method [40]. We then perform a Fourier transform to obtain the dynamical structure factor in momentum space, as described in Ref. [58]. Here, c denotes the site in the middle of the cluster, and the operator S^z_j measures the total z component of the spin on site j. The sum of the $S_{c,j}(\omega)$ contributions from sites on the same rung corresponds to a momentum transfer of $q_\perp = 0$ along the rung.

All numerical simulations are computed using the DMRG method [59,60], as implemented in the DMRG++ code [61]. For all DMRG simulations used in Bayesian optimization (BO), we use 16×2 clusters and keep up to $m = 2000$ states in both ground state and dynamical runs. The broadening parameter $\eta = 0.05t$ is set to match the experimental resolution. Calculations for $S(\mathbf{q},\omega)$ were performed on longer 64×2 ladders and also kept $m = 2000$ states with a broadening of $\eta = 0.1t$.

We extracted the values of $t_\perp$ and t' from the RIXS data using the BO technique, a machine learning approach to find the global extrema of functions whose form is otherwise unknown [62]. Since the $S(\boldsymbol{q},\omega)$ depends nontrivially on the underlying Hamiltonian, BO is uniquely suited to tune for its parameters provided we define an appropriate cost function for the minimization. Here we choose

$$C = L_2[S_{\mathrm{expt}}(\boldsymbol{q},\omega) - S'_{\mathrm{theory}}(\boldsymbol{q},\omega)], \tag{A4}$$

where L_2 is the square root of the sum of the squared vector values obtained, and $S'(\boldsymbol{q},\omega)_{\mathrm{theory}}$ is the DMRG spectra interpolated onto the experimental grid. We use only the spectra with $\boldsymbol{q} > 0$ in our analysis. To apply BO, we use the *suggest* utility in the BAYESIANOPTIMIZATION [63] package. For each value of the cost function we report for a particular set of parameters, the optimizer suggests a new set. We iterate this process until the suggestions converge. The best-fit values are given in the article.

b. Binding energy

We compute the binding energy (BE) for the hole-doped 64×2 ladders using

$$\mathrm{BE} = 2E_{\mathrm{GS}}(N-1) - E_{\mathrm{GS}}(N) - E_{\mathrm{GS}}(N-2), \tag{A5}$$

where E_{GS} is the ground state energy and $N = 120$ is the number of electrons. We keep all other parameters unchanged. Per our definition, $\mathrm{BE} > 0$ indicates hole pairing.

[1] M. R. Norman, *The challenge of unconventional superconductivity*, Science **332**, 196 (2011).

[2] D. J. Scalapino, *A common thread: The pairing interaction for unconventional superconductors*, Rev. Mod. Phys. **84**, 1383 (2012).

[3] D. P. Arovas, E. Berg, S. A. Kivelson, and S. Raghu, *The Hubbard model*, Annu. Rev. Condens. Matter Phys. **13**, 239 (2022).

[4] S. R. White, D. J. Scalapino, R. L. Sugar, E. Y. Loh, J. E. Gubernatis, and R. T. Scalettar, *Numerical study of the two-dimensional Hubbard model*, Phys. Rev. B **40**, 506 (1989).

[5] E. Gull, M. Ferrero, O. Parcollet, A. Georges, and A. J. Millis, *Momentum-space anisotropy and pseudogaps: A comparative cluster dynamical mean-field analysis of the doping-driven metal-insulator transition in the two-dimensional Hubbard model*, Phys. Rev. B **82**, 155101 (2010).

[6] E. W. Huang, C. B. Mendl, H.-C. Jiang, B. Moritz, and T. P. Devereaux, *Stripe order from the perspective of the Hubbard model*, npj Quantum Mater. **3**, 22 (2018).

[7] M. Qin, T. Schäfer, S. Andergassen, P. Corboz, and E. Gull, *The Hubbard model: A computational perspective*, Annu. Rev. Condens. Matter Phys. **13**, 275 (2022).

[8] E. Gull, O. Parcollet, and A. J. Millis, *Superconductivity and the pseudogap in the two-dimensional Hubbard model*, Phys. Rev. Lett. **110**, 216405 (2013).

[9] B.-X. Zheng *et al.*, *Stripe order in the underdoped region of the two-dimensional Hubbard model*, Science **358**, 1155 (2017).

[10] M. Qin, C. M. Chung, H, Shi, E. Vitali, C. Hubig, U. Schollwock, S. R. White, and S. Zhang, *Absence of superconductivity in the pure two-dimensional Hubbard model*, Phys. Rev. X **10**, 031016 (2020).
[11] X. Dong, E. Gull, and A. J. Millis, *Quantifying the role of antiferromagnetic fluctuations in the superconductivity of the doped Hubbard model*, Nat. Phys. **18**, 1293 (2022).
[12] H.-C. Jiang and T. P. Devereaux, *Superconductivity in the doped Hubbard model and its interplay with next-nearest hopping t'*, Science **365**, 1424 (2019).
[13] S. Johnston, F. Vernay, B. Moritz, Z. X. Shen, N. Nagaosa, J. Zaanen, and T. P. Devereaux, *Systematic study of electron-phonon coupling to oxygen modes across the cuprates*, Phys. Rev. B **82**, 064513 (2010).
[14] M. Jiang, *Enhancing d-wave superconductivity with nearest-neighbor attraction in the extended Hubbard model*, Phys. Rev. B **105**, 024510 (2022).
[15] L. Zhang, T. Guo, Y. Mou, Q. Chen, and T. Ma, *Enhancement of d-wave pairing in the striped phase with nearest neighbor attraction*, Phys. Rev. B **105**, 155154 (2022).
[16] C. Peng, Y. Wang, J. Wen, Y. S. Lee, T. P. Devereaux, and H. C. Jiang, *Enhanced superconductivity by near-neighbor attraction in the doped extended Hubbard model*, Phys. Rev. B **107**, L201102 (2023).
[17] Z. Zhou, W. Ye, H.-G. Luo, J. Zhao, and J. Chang, *Robust superconducting correlation against intersite interactions in the extended two-leg Hubbard ladder*, Phys. Rev. B **108**, 195136 (2023).
[18] E. Dagotto, *Experiments on ladders reveal a complex interplay between a spin-gapped normal state and superconductivity*, Rep. Prog. Phys. **62**, 1525 (1999).
[19] T. Vuletić *et al.*, *The spin-ladder and spin-chain system $(La, Y, Sr, Ca)_{14}Cu_{24}O_{41}$: Electronic phases, charge and spin dynamics*, Phys. Rep. **428**, 169 (2006).
[20] P. Abbamonte *et al.*, *Crystallization of charge holes in the spin ladder of $Sr_{14}Cu_{24}O_{41}$*, Nature (London) **431**, 1078 (2004).
[21] M. Uehara *et al.*, *Superconductivity in the ladder material $Sr_{0.4}Ca_{13.6}Cu_{24}O_{41.84}$*, J. Phys. Soc. Jpn. **65**, 2764 (1996).
[22] T. Nagata *et al.*, *Pressure-induced dimensional crossover and superconductivity in the hole-doped two-leg ladder compound $Sr_{14-x}Ca_xCu_{24}O_{41}$*, Phys. Rev. Lett. **81**, 1090 (1998).
[23] E. Arrigoni, E. Fradkin, and S. A. Kivelson, *Mechanism of high-temperature superconductivity in a striped Hubbard model*, Phys. Rev. B **69**, 214519 (2004).
[24] H.-C. Jiang and S. A. Kivelson, *Stripe order enhanced superconductivity in the Hubbard model*, Proc. Natl. Acad. Sci. U.S.A. **119**, e2109406119 (2022).
[25] J. Tranquada *et al.*, *Quantum magnetic excitations from stripes in copper oxide superconductors*, Nature (London) **429**, 534 (2004).
[26] J. M. Tranquada, *Cuprate superconductors as viewed through a striped lens*, Adv. Phys. **69**, 437 (2020).
[27] R. Zhou *et al.*, *Signatures of two gaps in the spin susceptibility of a cuprate superconductor*, Nat. Phys. **21**, 97 (2025).
[28] E. Dagotto, J. Riera, and D. Scalapino, *Superconductivity in ladders and coupled planes*, Phys. Rev. B **45**, 5744 (1992).
[29] M. Troyer, H. Tsunetsugu, and T. M. Rice, *Properties of lightly doped t-J two-leg ladders*, Phys. Rev. B **53**, 251 (1996).
[30] S. Liu, H-C. Jiang, and T. P. Devereaux, *Nature of a single doped hole in two-leg Hubbard and t-J ladders*, Phys. Rev. B **94**, 155149 (2016).
[31] U. Kumar, A. Nocera, E. Dagotto, and S. Johnston, *Theoretical study of the spin and charge dynamics of two-leg ladders as probed by resonant inelastic x-ray scattering*, Phys. Rev. B **99**, 205130 (2019).
[32] N. Nücker *et al.*, *Hole distribution in $(Sr, Ca, Y, La)_{14}Cu_{24}O_{41}$ ladder compounds studied by x-ray absorption spectroscopy*, Phys. Rev. B **62**, 14384 (2000).
[33] T. Osafune, N. Motoyama, H, Eisaki, and S. Uchida, *Optical study of the $Sr_{14-x}Ca_xCu_{24}O_{41}$ system: Evidence for hole-doped Cu_2O_3 ladders*, Phys. Rev. Lett. **78**, 1980 (1997).
[34] See Supplemental Material at http://link.aps.org/supplemental/10.1103/PhysRevX.15.021049 for characterization of hole doping and charge order, analysis of RIXS spectra, and details of DMRG calculations.
[35] M. M. Sala *et al.*, *Energy and symmetry of dd excitations in undoped layered cuprates measured by Cu L_3 resonant inelastic x-ray scattering*, New J. Phys. **13**, 043026 (2011).
[36] Y. Wang, G. Fabbris, M. P. M. Dean, and G. Kotliar, *EDRIXS: An open source toolkit for simulating spectra of resonant inelastic x-ray scattering*, Comput. Phys. Commun. **243**, 151 (2019).
[37] J. Schlappa *et al.*, *Collective magnetic excitations in the spin ladder $Sr_{14}Cu_{24}O_{41}$ measured using high-resolution resonant inelastic x-ray scattering*, Phys. Rev. Lett. **103**, 047401 (2009).
[38] Y. Tseng *et al.*, *Crossover of high-energy spin fluctuations from collective triplons to localized magnetic excitations in $Sr_{14-x}Ca_xCu_{24}O_{41}$ ladders*, npj Quantum Mater. **7**, 92 (2022).
[39] S. Notbohm *et al.*, *One-and two-triplon spectra of a cuprate ladder*, Phys. Rev. Lett. **98**, 027403 (2007).
[40] A. Nocera and G. Alvarez, *Spectral functions with the density matrix renormalization group: Krylov-space approach for correction vectors*, Phys. Rev. E **94**, 053308 (2016).
[41] S. Li, A. Nocera, U. Kumar, and S. Johnston, *Particle-hole asymmetry in the dynamical spin and charge responses of corner-shared 1D cuprates*, Commun. Phys. **4**, 217 (2021).
[42] Z. Chen *et al.*, *Anomalously strong near-neighbor attraction in doped 1D cuprate chains*, Science **373**, 1235 (2021).
[43] Y. Wang, Z. Chen, T. Shi, B. Moritz, Z. X. Shen, and T. P. Devereaux, *Phonon-mediated long-range attractive interaction in one-dimensional cuprates*, Phys. Rev. Lett. **127**, 197003 (2021).
[44] A. Lanzara *et al.*, *Evidence for ubiquitous strong electron–phonon coupling in high-temperature superconductors*, Nature (London) **412**, 510 (2001).
[45] Y. He *et al.*, *Rapid change of superconductivity and electron-phonon coupling through critical doping in* Bi-2212, Science **362**, 62 (2018).
[46] P. Adamus *et al.*, *Analogies of phonon anomalies and electronic gap features in the infrared response of*

$Sr_{14-x}Ca_xCu_{24}O_{41}$ *and underdoped* $YBa_2Cu_3O_{6+x}$, Rep. Prog. Phys. **86**, 044502 (2023).

[47] N. Derriche and G. Sawatzky, *Non-uniform and anisotropic electric polarizability resulting in pronounced local repulsion minima in high-temperature superconductors*, arXiv:2405.00787.

[48] M. Dolfi, B. Bauer, S. Keller, and M. Troyer, *Pair correlations in doped Hubbard ladders*, Phys. Rev. B **92**, 195139 (2015).

[49] J. Schlappa *et al.*, *Spin-orbital separation in the quasi-one-dimensional Mott insulator* Sr_2CuO_3, Nature (London) **485**, 82 (2012).

[50] K. Wohlfeld, S. Nishimoto, M. W. Haverkort, and J. van den Brink, *Microscopic origin of spin-orbital separation in* Sr_2CuO_3, Phys. Rev. B **88**, 195138 (2013).

[51] K. Wohlfeld, *Propagation of an orbiton in the antiferromagnets: Theory and experimental verification*, arXiv:1912.11363.

[52] K. I. Kugel and D. Khomskiĭ, *The Jahn-Teller effect and magnetism: Transition metal compounds*, Sov. Phys. Usp. **25**, 231 (1982).

[53] L. Martinelli *et al.*, *Collective nature of orbital excitations in layered cuprates in the absence of apical oxygens*, Phys. Rev. Lett. **132**, 066004 (2024).

[54] V. Bisogni *et al.*, *Orbital control of effective dimensionality: From spin-orbital fractionalization to confinement in the anisotropic ladder system* $CaCu_2O_3$, Phys. Rev. Lett. **114**, 096402 (2015).

[55] A. Scheie, P. Laurell, J. Thomas, V. Sharma, A. I. Kolesnikov, G. E. Granroth, Q. Zhang, B. Lake, M. Mihalik Jr., R. I. Bewley, R. S. Eccleston, J. Akimitsu, E. Dagotto, C. D. Batista, G. Alvarez, S. Johnston, and D. A. Tennant, *Cooper-pair localization in the magnetic dynamics of a cuprate ladder*, arXiv:2501.10296.

[56] S. Vanishri *et al.*, *Crystal growth and characterization of two-leg spin ladder compounds:* $Sr_{14}Cu_{24}O_{41}$ *and* $Sr_2Ca_{12}Cu_{24}O_{41}$, J. Cryst. Growth **311**, 3830 (2009).

[57] J. Etrillard, M. Braden, A. Gukasov, U. Ammerahl, and A. Revcolevschi, *Structural aspects of the spin-ladder compound* $Sr_{14}Cu_{24}O_{41}$, Physica (Amsterdam) **403C**, 290 (2004).

[58] A. Nocera, Y. Wang, N. D. Patel, G. Alvarez, T. A. Maier, E. Dagotto, and S. Johnston, *Doping evolution of charge and spin excitations in two-leg Hubbard ladders: Comparing DMRG and FLEX results*, Phys. Rev. B **97**, 195156 (2018).

[59] S. R. White, *Density matrix formulation for quantum renormalization groups*, Phys. Rev. Lett. **69**, 2863 (1992).

[60] S. R. White, *Density-matrix algorithms for quantum renormalization groups*, Phys. Rev. B **48**, 10345 (1993).

[61] G. Alvarez, *The density matrix renormalization group for strongly correlated electron systems: A generic implementation*, Comput. Phys. Commun. **180**, 1572 (2009).

[62] J. Snoek, H. Larochelle, and R. P. Adams, *Practical Bayesian optimization of machine learning algorithms*, arXiv:1206.2944.

[63] F. Nogueira, *Bayesian optimization: Open source constrained global optimization tool for Python* (2014), https://github.com/bayesian-optimization/BayesianOptimization.